Precision Interferometric Measurements of Mirror Birefringence in High-Finesse Optical Resonators

Adam J. Fleisher,[*] David A. Long, Qingnan Liu, and Joseph T. Hodges

National Institute of Standards and Technology,

Gaithersburg, Maryland 20899, USA

Abstract

High-finesse optical resonators found in ultrasensitive laser spectrometers utilize supermirrors ideally consisting of isotropic high-reflectivity coatings. Strictly speaking, however, the optical coatings are often non-uniformly stressed during the deposition process and therefore do possess some small amount of birefringence. When physically mounted the cavity mirrors can be additionally stressed in such a way that large optical birefringence is induced. Here we report a direct measurement of optical birefringence in a two-mirror Fabry-Pérot cavity with $R = 99.99\%$ by observing TEM_{00} mode beating during cavity decays. Experiments were performed at a wavelength of 4.53 μm, with precision limited by both quantum and technical noise sources. We report a splitting of $\delta_\nu = 618(1)$ Hz, significantly less than the intrinsic cavity linewidth of $\delta_\mathrm{cav} \approx 3$ kHz. With a cavity free spectral range of 96.9 MHz, the equivalent fractional change in mirror refractive index due to birefringence is therefore $\Delta n/n = 6.38(1) \times 10^{-6}$.

[*] adam.fleisher@nist.gov

I. INTRODUCTION

Many fields of physics, ranging from gravitational-wave detection to quantum electrodynamics, make use of the fundamental properties of optical resonators to perform basic and applied research. Optical clocks rely on stable reference cavities to reduce laser linewidth and therefore improve long-term coherence during the interrogation of narrow atomic transitions. Whispering gallery mode and Fabry-Pérot microresonators provide compact platforms for emerging sensor technology. In each of the above, detailed investigations of optical resonator response to different photon polarization states have made seminal contributions to their respective fields [1–10]. For the purposes of chemical and biochemical sensing, polarization rotation induced by molecules on or at a surface has been further enhanced by the inclusion of the target under test inside of an optical resonator [11–15].

In precision molecular spectroscopy, optical resonators are used to enhance the effective interaction pathlength between the circulating photons and a sample of interest [16]. This pathlength enhancement scales linearly with the resonator finesse, and therefore the most sensitive spectrometers utilize supermirrors with the lowest possible absorption and scattering losses, often $\leq 1 \times 10^{-4}$. In addition to absorption pathlength enhancement, optical resonators can also act to enhance phase shifts due to molecular dispersion. High-sensitivity dispersion spectroscopy also requires mirrors with very low loss [17–22].

Mirror losses can be measured by cavity ring-down spectroscopy (CRDS), where the rate at which photons leak from the optical resonator is proportional to the inverse of the resonator round-trip losses [23]. When there is no appreciable absorption by the intracavity medium, photons decay from the cavity exponentially with a time constant $\tau_0 = \bar{n}L[c(1 - R)]^{-1}$ where $\bar{n}$ is the refractive index of the medium, L is the cavity length, c is the speed of light in a vacuum, and R is the mirror power reflectivity. When intracavity absorption is introduced and increased, the measured cavity losses increase and τ decreases. Therefore, the sensitivity of CRDS to weak absorption is directly related to how precisely one can measure the exponential time constant τ.

Deviations from exponential behavior during CRDS can ultimately limit a given spectrometer's performance. Among possible sources of non-exponential behavior, some common examples include interference from higher-order transverse modes [24] and saturation of the intracavity absorption [25–28]. Perturbed cavity decays can also originate from small intrin-

sic birefringence found in all real supermirror coatings. Previous experiments have investigated mirror birefringence by observing changes in τ as a function of incident polarization [29, 30], by optical feedback [31], by ellipsometry [32–34], and by simultaneously locking two lasers of slightly different frequencies and orthogonal polarizations to the resonator [4].

Very recently, Dupré reported independent observations of beating in CRDS signals attributed to relatively strong mirror birefringence [35]. Given the signal-to-noise ratio on individual cavity decays reported by Dupré, beating due to interference between the cavity polarization eigenstates was only observed when the mirror birefringence was an order of magnitude larger than the cavity round-trip losses. Additionally, Dupré only investigated the response of their high-finesse optical resonator at a single, linear incident polarization, and thus the importance of the relative phase between the two eigenstates could not be realized. Excitation by a single linear polarization state also introduced a potential bias due to significant differences in the intracavity power at various analyzer angles. With a higher signal-to-noise ratio on the cavity decays and a more diverse set of incident polarization conditions, one could directly measure mirror birefringence via interferometry with significantly higher precision.

By performing CRDS with a high signal-to-noise ratio in the regime where cavity losses were greater than the round-trip phase retardance, we directly measured mirror birefringence via determination of the lowest-order transverse mode (TEM_{00}) splitting. A high-finesse optical resonator ($\mathcal{F} \approx 31\,000$) constructed using mid-infrared mirrors with observable birefringence resulted in a unique set of net slow and fast axes which supported orthogonal linear polarization states with slightly different resonant optical frequencies. We observed this small difference in optical frequencies as a beating during the cavity decays for specific input photon polarization states in the presence of appropriate polarization analysis. This method of determining the supermirror birefringence by a measurement of the beat frequency from TEM_{00} mode splitting was, in a sense, a form of birefringence interferometry [4]. Our high-precision CRDS approach had high sensitivity for small amounts of birefringence ($\leq 10^{-8}$) as well as more than three orders of magnitude of dynamic range. We also present a complementary generalized model for identifying an ideal input polarization state in order to optimize high-precision retrieval of the cavity decay time constant (and therefore cavity losses) even in the presence of significant mirror birefringence.

3

II. MODEL

Our model of supermirror birefringence in a high-finesse optical resonator begins with the projection of an electric field of arbitrary polarization onto an arbitrary set of spatially orthogonal axes 1 and 2:

$$E(t) = E_1(t) \exp[-i(\omega_1 t - \phi_1)]$$
$$+ E_2(t) \exp[-i(\omega_2 t - \phi_2)]. \tag{1}$$

Here, $E_1(t)$ and $E_2(t)$ are time-dependent electric field magnitudes, ω_1 and ω_2 are the optical angular frequencies of each field in radians ($\omega_1 = 2\pi\nu_1$ and $\omega_2 = 2\pi\nu_2$, respectively), and ϕ_1 and ϕ_2 are the phases of each optical field. Here, the natural choice for a basis set is the net slow and fast axes of our optical resonator under study, a linear combination of the slow and fast optical axes of each individual mirror with observable birefringence. We aim to measure the cavity decay after projection onto a linear polarization analyzer (PA) orientated at an angle γ relative to the cavity slow axis. The intensity of the decaying optical field incident on a photodetector after the PA is:

$$I(\gamma, t) = E(\gamma, t) E^*(\gamma, t)$$
$$= a_1 f_1 I_1(t) \cos^2(\gamma) + a_2 f_2 I_2(t) \sin^2(\gamma) \tag{2}$$
$$+ \sqrt{a_1 f_1 I_1(t) a_2 f_2 I_2(t)} \sin(2\gamma) \cos(\omega_b t - \delta_\phi),$$

where a_1 and a_2 are the fraction of light intensity propagating along the slow or fast axes (where $a_1 + a_2 = 1$), f_1 and f_2 are frequency-dependent mode coupling factors (where $f_1 + f_2 = 1$), $I_m(t) = I_0 \exp(-t/\tau_m)$ for $m = 1$ and 2, and ω_b and δ_ϕ are the difference in angular frequency and phase between the slow and fast electric fields, respectively. In the limit where the laser linewidth is much greater than both the cavity linewidth and the birefringence splitting (i.e., $\Delta\nu_{\text{laser}} \gg \delta_{\text{cav}}$ and $\gg \omega_b/(2\pi)$) on the timescale of cavity buildup, the frequency-dependent mode coupling factors become identical and constant. If in addition we consider the mirror reflectivity to be the same for both axes (i.e., $\tau_1 = \tau_2 \equiv \tau$), Eq. 2 simplifies to Eq. 3:

$$\frac{I(\gamma, t)}{I_0} = \exp(-t/\tau)[A(\gamma) + B(\gamma)\cos(\omega_b t - \delta_\phi)]. \tag{3}$$

The factors $A(\gamma)$ and $B(\gamma)$ depend upon the polarization state by which the optical cavity is excited. Here we investigate in detail two specific cases: excitation with circularly polarized

light and excitation with linearly polarized light. For circular excitation, $a_1 = a_2 = 1/2$ and the absolute difference in phase is $|\delta_\phi| = \pi/2$. Thus $A(\gamma) = 1$, $B(\gamma) = \sin(2\gamma)$, and $\delta_\phi = \pm\pi/2$ for left-hand (LH) and right-hand (RH) excitation, respectively. Equation 3 can then be further simplified using the small-angle approximation $\sin(\omega_b t) \approx \omega_b t$:

$$\frac{I(\gamma, t)}{I_0} = \exp[-t(1/\tau \mp B(\gamma)\omega_b)]. \tag{4}$$

In the limit of weak birefringence and using circular excitation, the cavity decay filtered by a linear PA will be nearly exponential with an effective time constant of $\tau_{\text{eff}}(\gamma) = \tau/(1 \mp B(\gamma)\omega_b\tau)$ for LH and RH excitation, respectively. The maximum fractional deviation from τ is then defined as

$$\frac{\Delta\tau}{\tau} = \frac{\tau_{\text{eff,max}} - \tau}{\tau} \approx \omega_b\tau. \tag{5}$$

For excitation with linearly polarized light, the following conditions are met: $\eta = \tan^{-1}(\sqrt{a_2/a_1})$ where η is the angle the incident linearly polarized field makes with the net slow axis, and $\delta_\phi = 0$. In each of the experiments described here using linearly polarized light, $\eta = \gamma$. Making the substitution, $A(\gamma) = \cos^4(\gamma) + \sin^4(\gamma)$ and $B(\gamma) = \sin^2(2\gamma)/2$, a similar expression to Eq. 4 can then be derived using the small-angle approximation $\cos(\omega_b t) \approx 1 - (\omega_b t)^2/2$:

$$\frac{I(\gamma, t)}{I_0} = \exp[-t/\tau - B(\gamma)(\omega_b t)^2/2]. \tag{6}$$

In SI units $I_0 = pc\epsilon_0 T_c(\langle I_{1,0}\rangle + \langle I_{2,0}\rangle)/2$, where the coefficient $p = 1/4$ or $p = 1/2$ for circular or linear excitation, respectively, ϵ_0 is the permittivity of free space, T_c is the overall efficiency with which the incident spectrum is transmitted by the optical resonator, and $\langle\rangle$ denotes an averaging over optical cycles. Since our cavity design does not allow for one mirror to be rotated in a systematic fashion relative to the other, we must describe the two-mirror optical resonator as a whole, and thus only model net cavity birefringence.

The above expressions provide an intuitive, parameterized description of a single-mode cavity decay with TEM$_{00}$ mode beating that arises from the presence of mirror birefringence. An expression similar to Eq. 3 was reported by Stamataki et al. to qualitatively describe the signals observed during pulsed evanescent-wave cavity ring-down ellipsometry (EW-CRDE) [13]. An independent frequency-domain derivation by Dupré, equivalent by convolution theorem to our time-domain approach, also resulted in an expression similar to our generalized Eq. 3 [35]. As evidenced by the experiments reported here, our more general time-domain

5

approach quantitatively described cavity excitation by both circularly and linearly polarized light without ignoring polarization-dependent loss. We also introduce frequency-dependent mode coupling factors that, for the case of a swept laser-cavity locking scheme, renders these analytical expressions useful for cases of both weak and strong birefringence (relative to the round-trip cavity losses).

A Jones matrix description of the polarization state propagation for an arbitrary number of cavity round-trips was given by Huang and Lehmann in Eqs. 1-6 of Ref. [30]. In that formalism, the two TEM_{00} modes are the two eigenvalues of the Jones matrix $\boldsymbol{M}$. Using the cavity round-trip $\boldsymbol{M}$ which they derived, we can model the cavity decay at each time t after being pumped by light of arbitrary polarization as

$$v(t) = \boldsymbol{A}\boldsymbol{M}^{t/t_r}u, \tag{7}$$

where $\boldsymbol{A}$ is the Jones matrix for the PA, $t_r = 2\bar{n}L/c$ is the cavity round-trip time, and u is the vector describing the polarization state of the incident electric field in the laboratory xyz frame. An illustration of the two-mirror Fabry-Pérot cavity along with the coordinate system and variables introduced above is shown in Fig. 1. The Jones matrix for the PA as well as the Jones vectors for LH circularly polarized, RH circularly polarized, and linearly (lin) polarized light, respectively, are shown in Eqs. 8-11 [36]:

$$\boldsymbol{A} = \begin{bmatrix} \cos^2(\theta) & \cos(\theta)\sin(\theta) \\ \cos(\theta)\sin(\theta) & \sin^2(\theta) \end{bmatrix}, \tag{8}$$

$$u_{\text{LH}} = \frac{1}{\sqrt{2}} \begin{bmatrix} 1 \\ i \end{bmatrix}, \tag{9}$$

$$u_{\text{RH}} = \frac{1}{\sqrt{2}} \begin{bmatrix} 1 \\ -i \end{bmatrix}, \text{ and} \tag{10}$$

$$u_{\text{lin}} = \begin{bmatrix} \cos(\theta) \\ \sin(\theta) \end{bmatrix}. \tag{11}$$

In Eq. 8, we define θ as the angle the PA makes with the x-axis in the laboratory frame ($\theta = \alpha + \gamma$, where α is the angle the slow axis makes with the x-axis). In all linear polarization experiments reported here, both the input polarization vector and the PA are set at angles equal to θ (i.e., $\eta = \gamma$ as stated previously).
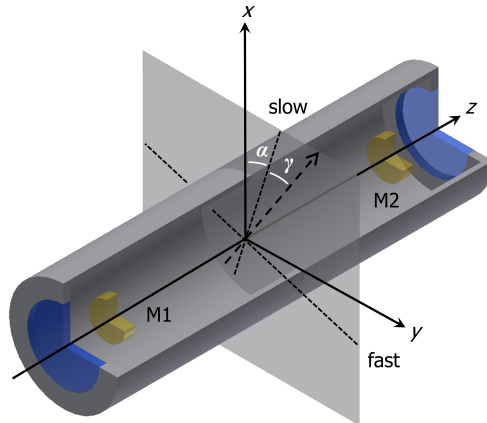
6

FIG. 1. (color online) Illustration of the high-finesse optical cavity. Supermirrors are label M1 and M2. CaF_2 windows with anti-reflective coating (blue) isolate the optical cavity from the laboratory. Net slow and fast optical axes are illustrated using dashed lines, and the linear polarization analyzer (PA) orientation using a dashed arrow. The angle between the slow axis and the x-axis is defined as α, whereas the angle between the slow axis and the PA is defined as γ. When studying the cavity response to linear excitation, the angle η that the incident linearly polarized light makes with the slow axis (not shown) is equal to γ.

Finally, the normalized intensity of the cavity decay incident on the photodetector at a given time t is equal to

$$\frac{I(t)}{I_0} = |v(t) \cdot v^*(t)|. \tag{12}$$

The cavity round-trip Jones matrix $\boldsymbol{M}$ contains the following parameters: the round-trip phase retardance $\epsilon = \omega_b t_r / 2$ and the angle α the slow axis makes with the x-axis in the laboratory frame. We can now make a connection between the perturbed exponential expressions derived above from an intuitive description of transverse mode beating and the Jones matrix approach. Through Eq. 5 and the above definition of round-trip phase retardance, we find for excitation of the cavity by circular polarization that $\Delta\tau/\tau = \epsilon/(1-R)$ in the limit of weak birefringence. In its general form, $\boldsymbol{M}$ also treats polarization-dependent loss in each cavity mirror, a small perturbation on supermirror birefringence that has not be included in Eqs. 3-6. We will revisit this topic later.
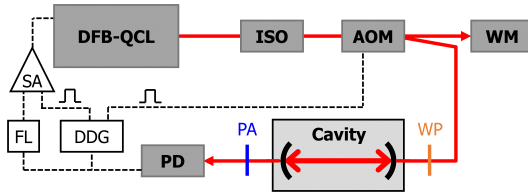
7

FIG. 2. (color online) Diagram of the cavity ring-down spectrometer. The optical components (dark gray boxes) are: DFB-QCL, distributed feedback quantum cascade laser; ISO, optical isolator; AOM, acousto-optic modulator; WM, wavelength meter; and PD, photodetector. Also shown are a waveplate (WP, orange) and linear polarization analyzer (PA, blue). Electronic components (white boxes) are: DDG, digital delay generator; FL, feedback loop; and SA, summing amplifier. Free-space laser propagation is shown as solid red lines, whereas electronic cables are shown as black dashed lines. TTL signals responsible for optical switching are illustrated where appropriate.

III. INSTRUMENTATION

A schematic of the instrument designed to perform ultrasensitive cavity ring-down spectroscopy (CRDS) in the mid-infrared spectral region [37] is shown in Fig. 2. The optical cavity was excited by a continuous-wave distributed feedback quantum cascade laser (QCL) operating at 4.53 μm and with an average output power of $\approx$ 30 mW. The polarization state of the QCL output is linear. A germanium acousto-optic modulator (AOM) was used as a fast optical switch to initiate cavity decays while a low-bandwidth ($\approx$ 4 Hz) transmission lock maintained resonance between the single-frequency QCL and a given mode of the optical cavity by feeding back to the laser current. A low noise liquid-N_2-cooled InSb photodetector of 100 μm diameter with transimpedance gain of 1×10^6 V/A, responsivity of 3.7 A/W, and a 1 MHz bandwidth was used to record individual cavity decay events with a measured noise-equivalent power of 70 fW Hz$^{-1/2}$. The decays were digitized with 22-bit resolution at a sampling rate of 1 MS/s and a 3 dB electronic bandwidth of 480 kHz.

The high-finesse optical resonator under interrogation consisted of two mirrors from the same batch coated for maximum power reflectivity R at a wavelength of 4.6 μm (CRD Optics 901-0008-4600). The mirrors were created using ZnSe substrates of the following dimensions: a thickness of 5 mm, a diameter of 2 cm, and a radius of curvature of 1 m. The mirrors were glued to 2.54 cm outer diameter (OD) adapter rings using standard two-part epoxy and then

mounted inside a threaded stainless steel knife-edge flange using a single aluminum retaining ring. Each of the two mirror mounts was adjusted using high-thread-count set screws to aid in initial alignment of the optical cavity. The optical cavity length was $L = 1.55$ m, and the round-trip absorption and scattering losses were measured to be 1×10^{-4}.

The individual mirror mounts were supported by stainless steel brackets, each of which was connected to the other by four 2.54 cm OD Invar-36 rods. The mirror mounts themselves were connected by a stainless steel tube of 1.27 cm OD and a stainless steel bellows to reduce strain in the event of slow drifts in cavity length due to room temperature fluctuations. This tube housed the optical mode as well as any sample gas under study. Each mirror mount was capped with a CaF_2 window with anti-reflective coatings which sealed the entire optical cavity from the laboratory environment. The mirrors in this design experience a zero pressure difference between their anti-reflective and reflective faces, significantly reducing the potential for stress-induced birefringence [30, 35]. All experiments were performed under the vacuum of a turbomolecular pump at pressures < 1.3 Pa.

IV.   RESULTS AND DISCUSSION

Presented first are the results of exciting the two-mirror optical cavity with circularly polarized light. A quarter-wave plate (Altechna 2-IRPW-L/4-4500-C) and a high-contrast PA (ISP Optics POL-1.5-5-SI, extinction $\geq 10\,000 : 1$) were placed at positions WP and PA as illustrated in Fig. 2, respectively. For each of two orientations of the quarter-wave plate (LH and RH circular) we recorded cavity decay events at various linear projection angles $\theta = \alpha + \gamma$ defined by the PA. Decay signals were recorded at a constant trigger threshold of 150 mV which allowed for a 3 s total acquisition time at rates that ranged from 2 Hz to 14 Hz.

At each angle θ the average empty-cavity decay constant τ_{eff} for a 3 s acquisition ensemble is plotted in Fig. 3 for both LH (blue circles) and RH (black diamonds) circularly polarized excitation. A constant offset was subtracted from each individual cavity decay, which was then fit to a single exponential decay constant, τ_{eff}, and a floated amplitude using a non-linear-least-squares Levenberg-Marquardt algorithm [38].

For each respective handedness, the LH and RH data sets were fit to the model $\tau_{\mathrm{eff}}(\theta) = \tau[(1 \mp \omega_b \tau \sin[2(\theta - \alpha)])]^{-1}$, where $\omega_b = 2\pi \delta_\nu$. The fit parameters from Fig. 3 were $\tau =$
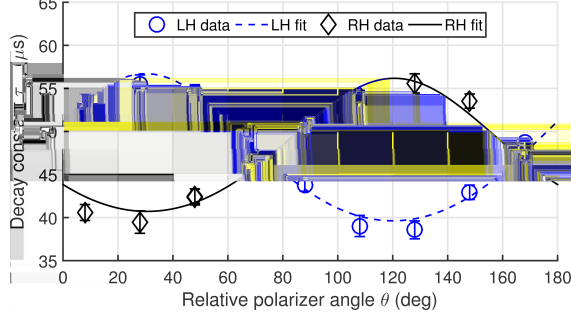
FIG. 3. (color online) The effective cavity decay time constant τ_{eff} as a function θ, the angle defined by the PA relative to the laboratory x-axis. Expanded uncertainties ($\pm 3\sigma$) for each 3 s acquisition. Repeated measurements are plotted at $\theta = 48°$ for each LH and RH data set to illustrate θ modulo $180°$ reproducibility.

46.7(4) μs, $\delta_\nu = 600(40)$ Hz, and $\alpha = -14.9(1.7)°$ for the LH data set and $\tau = 47.2(4)$ μs, $\delta_\nu = 540(40)$ Hz, and $\alpha = -14(2)°$ for the RH data set, respectively. From the model parameters averaged over both data sets we determined $\tau = 46.9(3)$ μs, $\delta_\nu = 570(30)$ Hz, and $\alpha = -14.7(1.5)°$.

Of the fit τ_{eff} in Fig. 3, the LH excitation data point at $\theta = 168°$ exhibited the smallest relative standard deviation of $\sigma_\tau = 0.044$ μs. This led to minimum observed fit statistics of $\sigma_\tau/\tau = 0.09$ %, about a factor of three from the theoretical value of $\sigma_\tau/\tau = 0.027$ % (the quadrature sum of the quantum noise $\sigma_\tau/\tau = 0.011$ % and the detector noise $\sigma_\tau/\tau = 0.025$ %, respectively) calculated when $\bar{I}_0 = 81(10)$ nW of light was incident on the photodetector ($\bar{I}_0$ was the average of all data reported in Fig. 3, with $\pm 1\sigma$ standard deviation in paren-thesis) [37, 39]. All decays were fit beginning 20 μs after the AOM optical switch to avoid occurrences of spurious optical pumping of the cavity as well as to reduce the influence of higher order transverse modes.

We now compare in detail the observed cavity decays when σ_τ is at its extrema. Figure 4 shows the measured cavity decays along with the corresponding fit residuals arising from three decay models: the single-exponential model (SEM) using τ_{eff}, the non-exponential model (NEM) of Eq. 3, and the Jones matrix model (JMM) of Eq. 7 and Eq. 12 in the limit of no polarization-dependent loss (PDL). For LH excitation, exponential decays at three distinct values of θ are plotted in Fig. 4A. Each of these decays were fitted by the SEM (solid circles in Fig. 4B-D), the NEM (open squares), and the JMM (small dots). For the
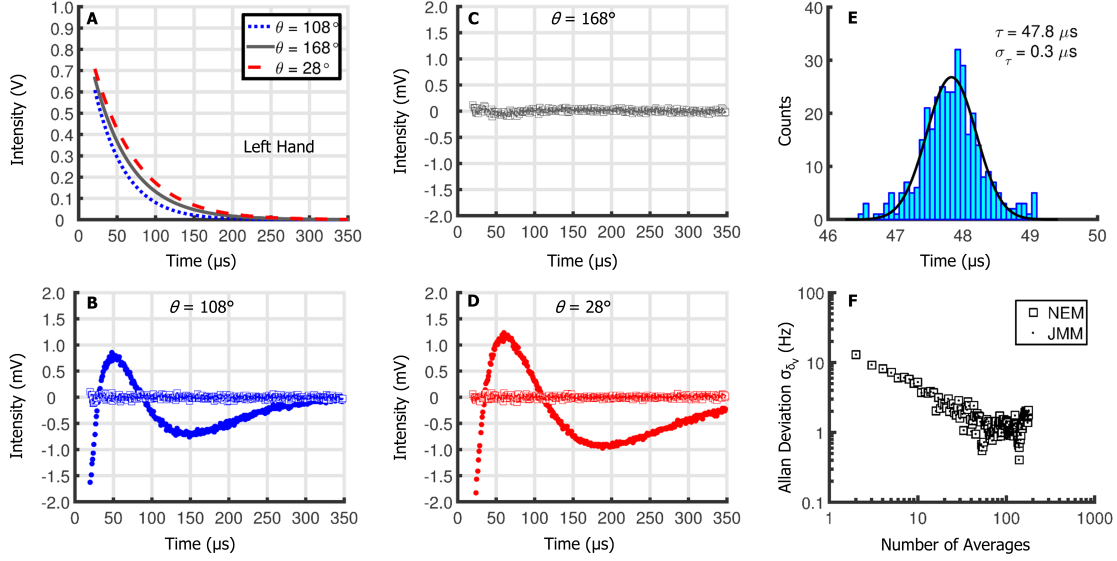
FIG. 4. (color online) A. Cavity decays at various angles θ for LH excitation. B-D. Fit residuals from the single exponential model (SEM, solid circles), the non-exponential model (NEM, open squares), and the Jones matrix model (JMM, small dots). The NEM and JMM residuals are identical for all θ. E. Histogram of the fitted τ from the JMM for 346 unique cavity decays recorded at 5 different values of θ for LH and RH excitation separated into 35 bins. A fitted normal distribution is shown as a solid black line. The histogram of fitted τ values using the NEM is identical (not shown). F. Allan deviation of fitted δ_ν for linear excitation at $\theta = 33°$ recorded at an acquisition rate of 9 Hz.

NEM and JMM, $\alpha = -14.7°$ was held constant at all θ and an amplitude parameter, τ, and δ_ν were all floated during the fit. When $|\sin[2(\theta - \alpha)]|$ was at a maximum the SEM left large residuals, whereas the SEM did well when $|\sin[2(\theta - \alpha)]| \approx 0$ at $\theta \approx 168°$ (In Fig. 4C, the solid circles of the SEM, effectively identical to the NEM and JMM, are obscured from view). While the SEM failed to model the cavity decays at all θ, the NEM and JMM are indistinguishable from one another, and performed well over all θ. A similar pattern was observed for RH excitation (not shown).

At each value of θ, the NEM and JMM provided fitted values for the amplitude of the decay, a single global time constant τ, and the beat frequency δ_ν. A histogram plot in Fig. 4E shows the ensemble of fitted τ values acquired at all θ where a beat was observed. The τ values are well approximated by a normal distribution with $\tau = 47.8$ μs and $\sigma_\tau = 0.3$ μs

(identical for both the NEM and JMM). For the same decays, the ensemble of fitted values of $\delta_\nu = 600$ Hz exhibit a larger relative standard deviation of $\sigma_{\delta_\nu} = 60$ Hz. For the two angles of θ measured in the lab with the largest perturbation from birefringence ($\theta = 28°$ and $128°$, respectively) and therefore the largest signal-to-noise ratio on the beat, we measure $\delta_\nu = 610$ Hz and $\sigma_{\delta_\nu} = 30$ Hz. At $\theta = 28°$ following LH circular excitation the perturbation from birefringence is near maximum, since $\theta \approx \alpha$. At an acquisition rate of 9 Hz, we report a measurement precision of $\sigma_{\delta_\nu} = 6$ Hz in 1 s of averaging on a measured value of $\delta_\nu = 613$ Hz.

Excitation of the cavity by linear polarization can also be treated by both the NEM and JMM using the appropriate coefficients $A(\gamma)$ and $B(\gamma)$ in Eq. 3. When $\eta = \gamma$, rotating η and γ together is equivalent to rotating the cavity itself relative to a fixed linear polarization. We note that, at a constant trigger threshold, this approach does not suffer from any potential bias due to changes in the intracavity power as a function of the angle of the linear polarization analyzer [35]. Exciting the cavity at $\theta = 33°$ (near where $\Delta\tau/\tau$ for circular polarization in Fig. 3 was largest) results in decays with the largest deviation from the SEM. The measured beat frequency at $\theta = 33°$ is $\delta_\nu = 618$ Hz with an improved precision of $\sigma_{\delta_\nu} = 1$ Hz due to a the longer 19 s acquisition time (see Fig. 4F). With a cavity free spectral range of FSR = 96.9 MHz, this equates to a measured fractional change in refractive index of $\Delta n/n = \delta_\nu/\text{FSR} = 6.38(1) \times 10^{-6}$. Precision on the 10^{-8} level is one order-of-magnitude better than that recently reported by Dupré for a cavity of $\mathcal{F} \approx 420\,000$ at a wavelength of 800 nm [35].

The Allan deviation for the linear excitation measurement (Fig. 4F) clearly demonstrated that averaging times > 10 s are possible. The agreement between the reported values of δ_ν for both circular and linear excitation given their respective values of σ_{δ_ν} is excellent when considering that these data sets were recorded several days apart. This suggests that long-term drift in the net cavity birefringence due to temperature changes in the laboratory are no more significant than our current short-term measurement precision.

In CRDS, we desire to simply avoid mirror birefringence altogether in order to achieve optimized fit statistics for the unperturbed cavity time constant τ. With knowledge of the spatial location of the slow and fast cavity axes in the laboratory frame we can selectively excite one of the modes and measure the Allan deviation to determine an NEA normalized to a 1 s acquisition. When $\theta = 168°$ ($\eta = \gamma \approx 3°$, $I_0 = 203$ nW) we report $\sigma_\tau/\tau = 0.024$ %

for the SEM, within a factor of two of the theoretical value of $\sigma_\tau/\tau = 0.012$ % calculated from the quadrature sum of quantum and technical noise when the fitting is performed with appropriate weighting (see Refs. [37, 39]). This results in an NEA $= 5.5 \times 10^{-11}$ cm^{-1} Hz$^{-1/2}$ at an acquisition rate of only 9 Hz. If in the laboratory the exact condition $\theta = \alpha$ (or $\theta = \alpha \pm 90°$) is met with excitation by linear polarization, we can indeed achieve the theoretical limit of σ_τ/τ set by both quantum and detector noise [37].

When $\epsilon < 1 - R$ (and therefore $\delta_\nu < \delta_{\mathrm{cav}}$) both the NEM and JMM perform equally well in the limit where PDL is negligible (and at the experimental signal-to-noise ratio on the cavity decays of SNR $\approx 3\,000 : 1$). In an effort to measure the PDL we have fit the average cavity decays at each value of θ for the LH and RH data sets to a global set of parameters that includes PDL in the JMM as described in Ref. [30]. Each averaged cavity decay was normalized by its previously fit amplitude and then collectively fit using the JMM+PDL with the following floated terms: τ, α, ϵ, b, and β, where $b = (r_{\mathrm{max}} - r_{\mathrm{min}})/(r_{\mathrm{max}} + r_{\mathrm{min}})$ (r is the net field reflectivity of the mirrors) and β is the angle r_{max} makes with the x-axis. We report $b/\epsilon = 0.057(16)$ with $\beta = 17(12)°$ and $b/\epsilon = 0.09(7)$ with $\beta = 60(20)°$ for the LH and RH data sets, respectively. Clearly PDL is a small perturbation on the mirror birefringence, and we can safely place an upper-bound of $b/\epsilon < 0.1$ on the net cavity PDL for this pair of mirrors. The simultaneous fit over all θ within a data set returns large uncertainties in β, again suggesting that PDL is small. PDL of this magnitude is consistent with previous observations in Ref. [30] as well as preliminary experiments on our existing near-infrared supermirrors.

When $\epsilon \approx 1 - R$, the round-trip phase retardance of the optical resonator is equal to the round-trip losses. This leads to a TEM$_{00}$ mode splitting that approaches the cavity linewidth ($\delta_\nu \approx \delta_{\mathrm{cav}}$), necessitating frequency-dependent mode coupling factors f_1 and f_2 in the NEM when a narrow linewidth continuous-wave laser is coupled to the optical resonator (see Eq. 2 and the surrounding text). In this strong birefringence regime ($\delta_\nu \geq \delta_{\mathrm{cav}}$) we anticipate that f_1 and f_2 will change for every cavity decay recorded by our spectrometer due to the swept laser locking and thresholding used to trigger the optical switch. The small-angle approximations used to derive Eqs. 4-6 are not justified when $\epsilon \approx 1 - R$, and the SEM fails even more dramatically than shown in Fig. 4. The use of Eq. 5 to estimate ω_b from the SEM of decays following LH and RH excitation is no longer valid, and the full NEM or JMM must be applied. When $\delta_\nu \approx \delta_{\mathrm{cav}}$, $1/\omega_b \approx \tau$. Making the substitution into

Eq. 5, we see that $\Delta\tau/\tau \approx 1$ and cavity decays are expected to be far from exponential.

By replacing M1 of the optical resonator with a presumably identical supermirror we fortuitously observed strong net birefringence in the $\epsilon \approx 1 - R$ regime. For LH, RH, and linear excitation we identified several PA orientations in the laboratory frame where the SEM produced large fitted residuals. For 133 total cavity decays fitted by Eq. 2 (still under the assumption of no PDL, i.e. $\tau_1 = \tau_2 \equiv \tau$) at various θ we report $\delta_\nu = 3.1$ kHz with a standard deviation of 0.4 kHz. We observed a maximum deviation from the SEM for LH excitation at $\theta = 138°$ (i.e., $\alpha = 93°$), and proceeded to record 170 successive cavity decays at an acquisition rate of 17 Hz with the PA in that orientation. The average beat frequency for the $\theta = 138°$ data set was $\delta_\nu = 2.789$ kHz with 9 Hz precision at 5 s of averaging. An Allan plot revealed that the deviation of δ_ν remained inversely proportional to the $\sqrt{N}$, where N is the number of cavity decays, for a minimum of 5 s. Therefore, with longer averaging times it may be possible to again achieve ≤ 1 Hz precision even in the presence of strong mirror birefringence.

The origin of the observed strong mirror birefringence that coincided with replacing a single mirror of the optical resonator could be reasoned in one of two ways. Since we measured net birefringence, the new M1 could simply have significantly larger birefringence than the first M1. Alternatively, the relative orientations of α_{M1} and α_{M2} could be very different in the two optical resonators, meaning that in our first optical resonator with $\delta_\nu = 618$ Hz the slow and fast axes of the individual supermirrors were oriented close to $90°$ from one another in the laboratory frame. However, without the ability to rotate the individual supermirrors once the optical resonators were constructed, we cannot confirm which of these two scenarios correctly describes our observations.

V. OUTLOOK

A variety of physical measurements in optics and laser metrology require a detailed understanding of supermirror birefringence. By measuring cavity decays with a high signal-to-noise ratio, we show that mirror birefringence can be measured with 10^{-8} sensitivity and greater than 10^3 dynamic range via TEM_{00} mode interferometry using either a non-exponential model or a Jones-matrix model. In CRDS, deviations from exponential cavity decays lead directly to higher uncertainties in the fitted values of τ, thus limiting spectrom-

eter sensitivity. The model and measurements reported here allowed for an unambiguous determination of the optimum polarization conditions for ultrasensitive CRDS, a prerequisite determination for the quantitative measurement of ultra-trace gas species in the so-called "molecular fingerprint" region of the mid-infrared [37].

CRDS often uses optical isolators before and after the optical resonator in order to minimize long-term drifts in τ due to etaloning [40]. This should be done with an understanding that excess polarization rotation and analysis could lead to non-exponential decays, and again, degraded fit statistics. In the mid-infrared, care must also be taken during the choice of material for vacuum windows since common substrates could induce residual ellipticity to the polarization state of the photons incident on the optical resonator and thus further complicate the decay signals.

While a detailed understanding of mirror birefringence in high-finesse optical resonators will aid in the design of ultrasensitive cavity ring-down spectrometers, cavity-enhanced polarimetry (CEP) experiments may also benefit from similar precision measurements. Recent demonstrations of background-free CEP, where drifts in mirror birefringence are intentionally negated by the measurement scheme, have reported impressive observations of weak intracavity birefringence for the purpose of quantifying the Kerr effect in gases [41], for detecting parity-nonconserving optical rotation in metastable atoms [42], and for the measurement of optical activity in chiral molecules [43, 44]. In earlier implementations of CEP, however, mirror birefringence remained a significant source of non-negligible background signal [45–50]. In those experiments, detailed knowledge of mirror anisotropy and birefringence was required to properly interrogate the optical resonator thus minimizing background contributions to the overall detection of weak intracavity polarization effects. Using the high precision, large dynamic range interferometric detection method demonstrated here, CEP could also take advantage of immunity to laser intensity fluctuation and > 100 Hz acquisition rates commonly achieved in CRDS. Finally, the addition of a transverse magnetic field to the optical resonator could lead to high-precision measurements of the Voigt effect of gases by ultrasensitive ellipsometry.

ACKNOWLEDGMENTS

[1] J. B. Camp, W. Kells, M. M. Fejer, and E. Gustafson, Appl. Opt. **40**, 3753 (2001).

[2] P. Asenbaum and M. Arndt, Opt. Lett. **36**, 3720 (2011).

[3] H. Mabuchi, J. Ye, and H. Kimble, Appl. Phys. B **68**, 1095 (1999).

[4] J. L. Hall, J. Ye, and L.-S. Ma, Phys. Rev. A **62**, 013815 (2000).

[5] F. Brenneckei, T. Donner, S. Ritter, T. Bourdel, M. Köhl, and T. Esslinger, Nature **450**, 268 (2007).

[6] T. Kessler, C. Hagemann, C. Grebing, T. Legero, U. Sterr, F. Riehle, M. Martin, L. Chen, and J. Ye, Nature Photon. **6**, 687 (2012).

[7] G. Cole, W. Zhang, M. Martin, J. Ye, and M. Aspelmeyer, Nature Photon. **7**, 644 (2013).

[8] D. V. Strekalov, R. J. Thompson, L. M. Baumgartel, I. S. Grudinin, and N. Yu, Opt. Express **19**, 14495 (2011).

[9] A. Libson, N. Brown, A. Buikema, C. C. López, T. Dordevic, M. Heising, and M. Evans, Opt. Express **23**, 3809 (2015).

[10] M. Uphoff, M. Brekenfeld, G. Rempe, and S. Ritter, New J. Phys. **17**, 013053 (2015).

[11] A. Karaiskou, V. Papadakis, B. Loppinet, and T. P. Rakitzis, J. Chem. Phys. **131**, 121101 (2009).

[12] M. A. Everest, V. M. Papadakis, K. Stamataki, S. Tzortzakis, B. Loppinet, and T. P. Rakitzis, J. Phys. Chem. Lett. **2**, 1324 (2011).

[13] K. Stamataki, V. Papadakis, M. A. Everest, S. Tzortzakis, B. Loppinet, and T. P. Rakitzis, Appl. Opt. **52**, 1086 (2013).

[14] D. Sofikitis, K. Stamataki, M. A. Everest, V. Papadakis, J.-L. Stehle, B. Loppinet, and T. P. Rakitzis, Opt. Lett. **38**, 1224 (2013).

[15] D. Sofikitis, A. K. Spiliotis, K. Stamataki, G. E. Katsoprinakis, L. Bougas, P. C. Samartzis,

B. Loppinet, T. P. Rakitzis, M. Surligas, and S. Papadakis, Appl. Opt. **54**, 5861 (2015).

[16] G. Gagliardi and H. Loock, *Cavity-Enhanced Spectroscopy and Sensing*, Springer Series in Optical Sciences (Springer Berlin Heidelberg, 2013).

[17] J. Ye, L.-S. Ma, and J. L. Hall, J. Opt. Soc. Am. B **15**, 6 (1998).

[18] A. Foltynowicz, F. Schmidt, W. Ma, and O. Axner, Appl. Phys. B **92**, 313 (2008).

[19] A. Cygan, D. Lisak, P. Morzyński, M. Bober, M. Zawada, E. Pazderski, and R. Ciuryło, Opt. Express **21**, 29744 (2013).

[20] D. A. Long, G.-W. Truong, R. D. van Zee, D. F. Plusquellic, and J. T. Hodges, Appl. Phys. B **114**, 489 (2014).

[21] I. Silander, T. Hausmaninger, W. Ma, P. Ehlers, and O. Axner, Opt. Lett. **40**, 2004 (2015).

[22] A. Cygan, P. Wcisło, S. Wójtewicz, P. Masłowski, J. T. Hodges, R. Ciuryło, and D. Lisak, Opt. Express **23**, 14472 (2015).

[23] K. W. Busch and M. A. Busch, eds., *Cavity-Ringdown Spectroscopy* (American Chemical Society, Washington, DC, 1999).

[24] H. Huang and K. Lehmann, Opt. Express **15**, 8745 (2007).

[25] G. Giusfredi, S. Bartalini, S. Borri, P. Cancio, I. Galli, D. Mazzotti, and P. De Natale, Phys. Rev. Lett. **104**, 110801 (2010).

[26] I. Galli, S. Bartalini, S. Borri, P. Cancio, D. Mazzotti, P. De Natale, and G. Giusfredi, Phys. Rev. Lett. **107**, 270802 (2011).

[27] K. Lehmann, Appl. Phys. B **116**, 147 (2014).

[28] G. Giusfredi, I. Galli, D. Mazzotti, P. Cancio, and P. D. Natale, J. Opt. Soc. Am. B **32**, 2223 (2015).

[29] J. Y. Lee, H.-W. Lee, J. W. Kim, Y. S. Yoo, and J. W. Hahn, Appl. Opt. **39**, 1941 (2000).

[30] H. Huang and K. K. Lehmann, Appl. Opt. **47**, 3817 (2008).

[31] J. Morville and D. Romanini, Appl. Phys. B **74**, 495 (2002).

[32] D. Jacob, F. Bretenaker, P. Pourcelot, P. Rio, M. Dumont, and A. Doré, Appl. Opt. **33**, 3175 (1994).

[33] F. Bielsa, A. Dupays, M. Fouché, R. Battesti, C. Robilliard, and C. Rizzo, Appl. Phys. B **97**, 457 (2009).

[34] P. Berceau, M. Fouché, R. Battesti, F. Bielsa, J. Mauchain, and C. Rizzo, Appl. Phys. B **100**, 803 (2010).

[35] P. Dupré, Phys. Rev. A **92**, 053817 (2015).

[36] E. Hecht, *Optics*, 4th ed. (Pearson/Addison-Wesley, 2002).

[37] D. A. Long, A. J. Fleisher, Q. Lui, and J. T. Hodges, (unpublished).

[38] D. Halmer, G. von Basum, P. Hering, and M. Mürtz, Rev. Sci. Instrum. **75**, 2187 (2004).

[39] H. Huang and K. K. Lehmann, J. Phys. Chem. A **117**, 13399 (2013).

[40] J. Courtois and J. T. Hodges, Opt. Lett. **37**, 3354 (2012).

[41] M. Durand, J. Morville, and D. Romanini, Phys. Rev. A **82**, 031803 (2010).

[42] L. Bougas, G. E. Katsoprinakis, W. von Klitzing, J. Sapirstein, and T. P. Rakitzis, Phys. Rev. Lett. **108**, 210801 (2012).

[43] D. Sofikitis, L. Bougas, G. E. Katsoprinakis, A. K. Spiliotis, B. Loppinet, and T. P. Rakitzis, Nature **514**, 76 (2014).

[44] L. Bougas, D. Sofikitis, G. E. Katsoprinakis, A. K. Spiliotis, P. Tzallas, B. Loppinet, and T. P. Rakitzis, J. Chem. Phys. **143**, 104202 (2015).

[45] Y. Le Grand, M. Medjaou, A. Le Floch, and R. Le Naour, Appl. Phys. Lett. **51** (1987).

[46] Y. L. Grand and A. L. Floch, Opt. Lett. **17**, 360 (1992).

[47] R. Engeln, G. Berden, E. van den Berg, and G. Meijer, J. Chem. Phys. **107** (1997).

[48] J. Poirson, M. Vallet, F. Bretenaker, A. L. Floch, and J.-Y. Thépot, Anal. Chem. **70**, 4636 (1998).

[49] M. Vallet, F. Bretenaker, A. L. Floch, R. L. Naour, and M. Oger, Opt. Commun. **168**, 423 (1999).

[50] T. Müller, K. B. Wiberg, and P. H. Vaccaro, J. Phys. Chem. A **104**, 5959 (2000).